Variable-Speed Control of a Six-Phase Induction Machine using Predictive-Fixed Switching Frequency Current Control Techniques

Osvaldo Gonzalez[1], Magno Ayala[1], Jesus Doval-Gandoy[2], Jorge Rodas[1], Raul Gregor[1] and Gustavo Rivas[1]
[1]Laboratory of Power and Control Systems, Facultad de Ingeniería, Universidad Nacional de Asunción, Paraguay,
ogonzalez@ing.una.py, mayala@ing.una.py, jrodas@ing.una.py, rgregor@ing.una.py, gusyri@hotmail.com
[2]Applied Power Electronics Technology Research Group, Universidad de Vigo, Spain, jdoval@uvigo.es

***Abstract*—Model predictive control method has been recently introduced as an alternative to inner current controllers of multiphase drives using rotor field oriented control methods. Model predictive controllers are distinguished by a variable switching frequency which causes noise, large voltage and current ripples at low sampling frequency. Therefore, this paper proposes a variable-speed control for six-phase induction motor drives by using an inner loop of predictive-fixed switching frequency current control scheme. Experimental results are provided in order to prove the feasibility of the proposed control technique, considering mean squared error as well as the total harmonic distortion of the stator currents as figure of merit. The efficiency of the proposed control could be verified by applying the non-parametric Mann-Whitney statistical test on the experimentally obtained data.**

***Index Terms*—Fixed switching frequency, multiphase machines, predictive control.**

I. Introduction

Multiphase induction machine (IM) has gained higher attention compared to its three-phase counterparts due to its fault tolerance, lower torque pulsation and better power distribution per phase which are very attractive to the research community for industrial applications where a high-performance control is required [1]. In recent times, several applications of multiphase IMs are being studied, such as wind power generation system, electric vehicles (EV) and hybrid EV [2]. In all these applications, multiphase IM would be performed under variable-speed conditions, including speed sensorless operations [3]. The most common speed control structure for multiphase IM is the field-oriented control (FOC) technique, a cascaded scheme with an inner current control loop and an outer speed control loop [4]. Several new control strategies have been developed for the inner current control loop for multiphase IM such as: model predictive control (MPC), resonant and direct torque control and also its extension to post-fault operation [5]. The implemented solution of MPC shows excellent transient performance as well as the easy inclusion of nonlinearities in the model comparing with traditional proportional-integral (PI) controllers [6]. The main obstacle of the MPC methods is that the control can only select from a finite number of valid switching states because of the absence of a modulator. This generates distortion and also large voltage and current ripples at low sampling frequency. The variable switching frequency produces a spread spectrum, decreasing the performance of the system in terms of power quality [7]. To overcome this issue, an enhanced predictive controller with fixed switching frequency is presented in this paper. This method is based on a modulation scheme incorporated to the conventional MPC for different power converters [8]–[11]. This method is applied to a two-level voltage source inverter (VSI), where for a selected number of switching states the duty cycles are generated by using two active vectors and two zero vectors which are applied to the converter using a given switching pattern in order to obtain an efficient dynamic of the system. For the external speed control loop, a PI controller is designed by a technique detailed in [12].

The main contribution of this paper is the experimental validation of the aforementioned predictive-fixed switching frequency technique used as an inner current control applied to a variable-speed six-phase IM drive. The efficiency of the predictive-fixed current control technique is analyzed by using the mean square error (MSE) and the total harmonic distortion (THD) as indices of performance. The figures of merit used are not of constant magnitude. This is easily appreciated when a replication of the experiment is performed. In such cases, we have a probability distribution function for each variable considered (MSE and THD). When sample sizes are small it is more appropriate to make no assumption about the distribution of variables when comparisons are to be made. This results in the application of non-parametric statistical techniques [13]. Specifically, the Mann-Whitney test is used to compare the central tendencies of the values obtained through the experimental results for each scenario described in Section IV.

II. Six-Phase Induction Machine Drive

A six-phase IM associated with a six-phase VSI and a DC voltage source (V_{dc}) is considered where the phase propagation angles of this IM are:

$$[\theta_p] = \left[\begin{array}{cccccc} 0 & \frac{\pi}{6} & \frac{2\pi}{3} & \frac{5\pi}{6} & \frac{4\pi}{3} & \frac{3\pi}{2} \end{array}\right] \tag{1}$$

The electrical scheme of the VSI drive is shown in Fig. 1. The six-phase IM is a continuous system which can be described by a group of differential equations. By applying the vector space decomposition (VSD) technique [14], the

978-1-5386-6705-7/18/$31.00

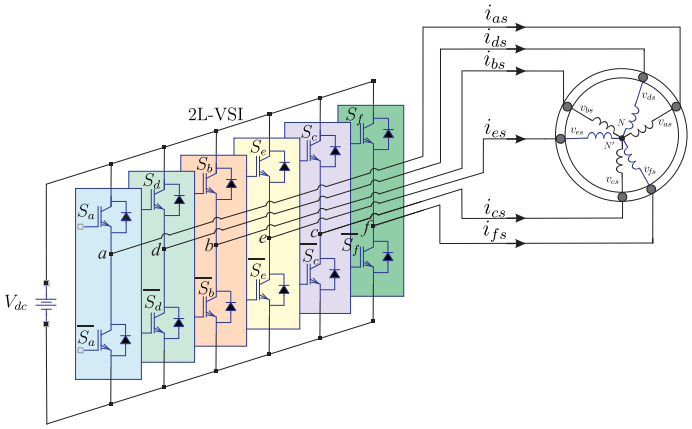

Fig. 1. Scheme of a six-phase IM connected to a six-phase VSI.

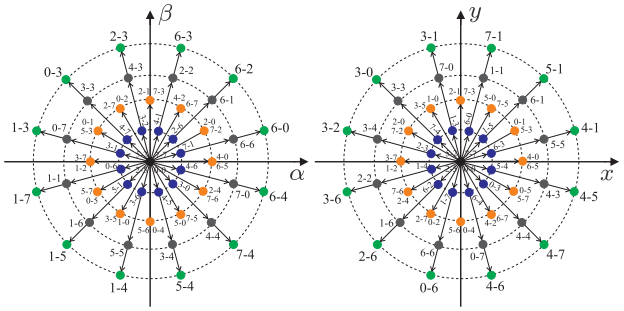

Fig. 2. Voltage space vectors and switching states in the (α-β) and (x-y) sub-spaces for a six-phase IM.

original six dimensional space of the six-phase IM, defined by its six phases (a, b, c, d, e, f), is converted into three two dimensional orthogonal sub-spaces in the stationary reference frame, represented as (α-β), (x-y) and (z_1-z_2), by using the transformation matrix $\mathbf{T}$ [15] and an invariant amplitude criterion was selected, where only (α-β) components contribute to the torque and flux production. The (z_1-z_2) components are not considered due to the isolated neutral points configuration.

$$\mathbf{T} = \frac{1}{3}\begin{bmatrix} \cos([\theta_p]) \\ \sin([\theta_p]) \\ \cos(5[\theta_p]) \\ \sin(5[\theta_p]) \\ 1 \;\; 0 \;\; 1 \;\; 0 \;\; 1 \;\; 0 \\ 0 \;\; 1 \;\; 0 \;\; 1 \;\; 0 \;\; 1 \end{bmatrix} \begin{matrix} \alpha \\ \beta \\ x \\ y \\ z_1 \\ z_2 \end{matrix} \tag{2}$$

The VSI has a discrete nature with an amount of $64 = 2^6$ different switching states defined by six switching functions corresponding to the six inverter legs $[S_a, S_b, S_c, S_d, S_e, S_f]$, where $\mathbf{S}_i \in \{0, 1\}$. The different switching states and the voltage of the V_{dc} define the phase voltages which can be mapped to the (α-β)-(x-y) sub-spaces according to the VSD approach. Fig. 2 shows the 64 possibilities which lead only to 48 different active voltage vectors plus one null vector in the (α-β)-(x-y) sub-spaces. The six-phase IM can be written by using a state-space model, based on the VSD technique and the dynamic reference transformation which is defined by:

$$\frac{d\mathbf{X}_{(t)}}{dt} = \mathbf{A}_{(t)}\,\mathbf{X}_{(t)} + \mathbf{B}_{(t)}\,\mathbf{U}_{(t)} + \mathbf{H}\,\varpi_{(t)} \tag{3}$$

being $\mathbf{U}_{(t)}$ the input vector of the state-space model, $\mathbf{X}_{(t)}$ the state vector and $\mathbf{A}_{(t)}$ and $\mathbf{B}_{(t)}$ are matrices determined by the electrical parameters of the six-phase IM. The process noise is defined as $\varpi_{(t)}$ and $\mathbf{H}$ is the noise weight matrix.

The state-space model, expressed in (3), and $\mathbf{X}_{(t)} = [x_1, x_2, x_3, x_4, x_5, x_6]^T$ defines the following equations:

$$\begin{aligned}
\frac{dx_1}{dt} &= -R_s c_2 x_1 + c_4\left(L_m\omega_r x_2 + R_r x_5 + L_r\omega_r x_6\right) + c_2 u_1 \\
\frac{dx_2}{dt} &= -R_s c_2 x_2 + c_4\left(-L_m\omega_r x_1 - L_r\omega_r x_5 + R_r x_6\right) + c_2 u_2 \\
\frac{dx_3}{dt} &= -R_s c_3 x_3 + c_3 u_3 \\
\frac{dx_4}{dt} &= -R_s c_3 x_4 + c_3 u_4 \\
\frac{dx_5}{dt} &= R_s c_4 x_1 + c_5\left(-L_m\omega_r x_2 - R_r x_5 - L_r\omega_r x_6\right) - c_4 u_1 \\
\frac{dx_6}{dt} &= R_s c_4 x_2 + c_5\left(L_m\omega_r x_1 + L_r\omega_r x_5 - R_r x_6\right) - c_4 u_2
\end{aligned} \tag{4}$$

where ω_r is the rotor electrical speed, R_s, R_r, L_m, $L_r = L_{lr} + L_m$ and $L_s = L_{ls} + L_m$ are the electrical parameters of the six-phase IM. The coefficients are determined as $c_1 = L_s L_r - L_m^2$, $c_2 = \frac{L_r}{c_1}$, $c_3 = \frac{1}{L_{ls}}$, $c_4 = \frac{L_m}{c_1}$ and $c_5 = \frac{L_s}{c_1}$. The input vector is constituted of the applied voltages to the stator $u_1 = v_{\alpha s}$, $u_2 = v_{\beta s}$, $u_3 = v_{xs}$, $u_4 = v_{ys}$ and the state vector corresponds to the six-phase IM stator and rotor currents $x_1 = i_{\alpha s}$, $x_2 = i_{\beta s}$, $x_3 = i_{xs}$, $x_4 = i_{ys}$, $x_5 = i_{\alpha r}$ and $x_6 = i_{\beta r}$.

Stator voltages are dependant of the input control signals. In this particular case, the simplest VSI model has been considered to achieve a good optimization process. Through this model the stator voltages can be obtained from the ideal six-phase VSI model $\mathbf{M}_{[\mathbf{S}]}$ [15].

$$\mathbf{M}_{[\mathbf{S}]} = \frac{1}{3}\begin{bmatrix} 2 & 0 & -1 & 0 & -1 & 0 \\ 0 & 2 & 0 & -1 & 0 & -1 \\ -1 & 0 & 2 & 0 & -1 & 0 \\ 0 & -1 & 0 & 2 & 0 & -1 \\ -1 & 0 & -1 & 0 & 2 & 0 \\ 0 & -1 & 0 & -1 & 0 & 2 \end{bmatrix} \mathbf{S}^T \tag{5}$$

Taking into account the ideal six-phase VSI, is possible to transform the gating signals into stator voltages which can be mapped to (α-β) and (x-y) sub-spaces and defined in $\mathbf{U}_{(t)} = [u_1, u_2, u_3, u_4]^T$ which yields to the following equations:

$$\mathbf{U}_{(t)} = V_{dc}\,\mathbf{T}\,\mathbf{M}_{[\mathbf{S}]} \tag{6}$$

$$\mathbf{Y}_{(t)} = \mathbf{C}\,\mathbf{X}_{(t)} + \nu_{(t)} \tag{7}$$

being $\mathbf{Y}$ the output vector, $\nu_{(t)}$ the measurement noise and $\mathbf{C}$:

$$\mathbf{C} = \begin{bmatrix} 1 & 0 & 0 & 0 & 0 & 0 \\ 0 & 1 & 0 & 0 & 0 & 0 \\ 0 & 0 & 1 & 0 & 0 & 0 \\ 0 & 0 & 0 & 1 & 0 & 0 \end{bmatrix}$$

The mechanical equations of the six-phase IM are:

$$T_e = 3P\left(\psi_{\alpha s} i_{\beta s} - \psi_{\beta s} i_{\alpha s}\right) \tag{8}$$

$$J_i \frac{d\omega_m}{dt} + B_i \omega_m = (T_e - T_L) \tag{9}$$

where B_i is the friction coefficient, J_i the inertia coefficient, T_e defines the generated torque, T_L is the load torque, ω_m is the rotor mechanical speed, $\psi_{\alpha s}$ and $\psi_{\beta s}$ are the stator fluxes, and P is the number of pole pairs.

III. Proposed Speed Controller

A two degree PI controller with saturator, proposed in [12], is utilized as the external speed control loop, based on FOC control technique due to its easiness. In the FOC scheme, PI speed controller is utilized to create the reference current in dynamic reference frame. The current reference utilized by the MPC are obtained from the calculation of the electric angle used to change the current reference, initially in dynamic reference frame (d-q), to static reference frame (α-β). The process of calculation of the slip frequency (ω_{sl}) is achieved in the same way as the FOC techniques, from the reference currents in dynamic reference frame (i^*_{ds}, i^*_{qs}) and the electrical parameters of the machine (R_r, L_r), and the mechanical speed is acquired by using an encoder. A detailed block diagram of the proposed speed control technique for the six-phase IM drive is presented in Fig. 3.

A. Classic MPC

MPC uses the mathematical model of the system, namely predictive model, to predict at time [k] the future values [k+1], by using measured variables such as the stator currents and the mechanical speed.

$$\hat{\mathbf{X}}_{[k+1|k]} = \mathbf{X}_{[k]} + T_s f\left(\mathbf{X}_{[k]},\, \mathbf{U}_{[k]},\, \omega_{r[k]}\right) \tag{10}$$

In the state-space representation (10) only the stator currents, voltages and mechanical speed are measured. The stator voltages are easily predicted from the switching commands issued to the VSI, however, the rotor currents cannot be directly measured. This fact can be solve by means of estimating the rotor current using a reduced order estimators where the reduced order estimators provide an estimate for only the unmeasured part of the state vector. Then, in this work, the rotor current is estimated by the method proposed in [16] by using a reduced order estimator based on a Kalman filter (KF). In that sense, considering a zero-mean Gaussian measurement and uncorrelated process noises, the system's equations can be written as:

$$\hat{\mathbf{X}}_{[k+1|k]} = \mathbf{A}_{[k]}\mathbf{X}_{[k]} + \mathbf{B}_{[k]}\mathbf{U}_{[k]} + \mathbf{H}\varpi_{[k]} \tag{11}$$

$$\mathbf{Y}_{[k+1|k]} = \mathbf{C}\,\mathbf{X}_{[k+1]} + \nu_{[k+1]} \tag{12}$$

where $\mathbf{A}_{[k]}$ and $\mathbf{B}_{[k]}$ are discretized matrices from (4). $\mathbf{A}_{[k]}$ depends on the present value of $\omega_{r[k]}$ and must be considered at every sampling time. A detailed description of the dynamics of the reduced order KF can be found in [16], [17] which has not been exhibit for the sake of conciseness.

B. Cost Function

Then, the MPC performs a optimization process at every sampling time. This process consists in the evaluation of a cost function (13) for all possible stator voltages in order to achieve its control objective. As the cost function can be represented in several ways, in this paper, it is selected the minimization of the current tracking error, defined as the following equation:

$$\begin{aligned} J_{[k+2|k]} =& \parallel i^*_{\alpha s[k+2]} - \hat{i}_{\alpha s[k+2|k]} \parallel^2 + \parallel i^*_{\beta s[k+2]} - \hat{i}_{\beta s[k+2|k]} \parallel^2 \\ &+ \lambda_{xy}\left(\parallel i^*_{xs[k+2]} - \hat{i}_{xs[k+2|k]} \parallel^2 + \parallel i^*_{ys[k+2]} - \hat{i}_{ys[k+2|k]} \parallel^2\right) \end{aligned} \tag{13}$$

being $i^*_{s[k+2]}$ the vector containing the reference for the stator currents and $\hat{i}_{s[k+2]}$ the vector containing the predictions based on the second-step ahead state. In order to put more emphasis on (α-β) or (x-y) sub-spaces a tuning parameter (λ_{xy}) is used [16], [17].

C. Modulated model predictive control (M2PC)

It is feasible to determine each available vector for the VSI in the (α-β) plane, which defines 64 sectors (48 different), which are given by two adjacent vectors. The proposed technique evaluates the prediction of the two active vectors that conform each sector at every sampling time and evaluates the cost function separately for each prediction. Each prediction is evaluated based on (10) and the only difference is in the calculation of the input vector $\mathbf{U}_{[k]}$ [15]. The duty cycles, for the two active vectors d_1 and d_2, are calculated by solving the following equations:

$$d_0 = \frac{\sigma}{J_0} \qquad d_1 = \frac{\sigma}{J_1} \qquad d_2 = \frac{\sigma}{J_2} \tag{14}$$

$$d_0 + d_1 + d_2 = T_s \tag{15}$$

where d_0 corresponds to the duty cycle of a zero vector. Then, it is possible to obtain the expression for σ and the duty cycles for each vector given as:

$$d_0 = \frac{T_s J_1 J_2}{J_0 J_1 + J_1 J_2 + J_0 J_2} \tag{16}$$

$$d_1 = \frac{T_s J_0 J_2}{J_0 J_1 + J_1 J_2 + J_0 J_2} \tag{17}$$

$$d_2 = \frac{T_s J_0 J_1}{J_0 J_1 + J_1 J_2 + J_0 J_2} \tag{18}$$

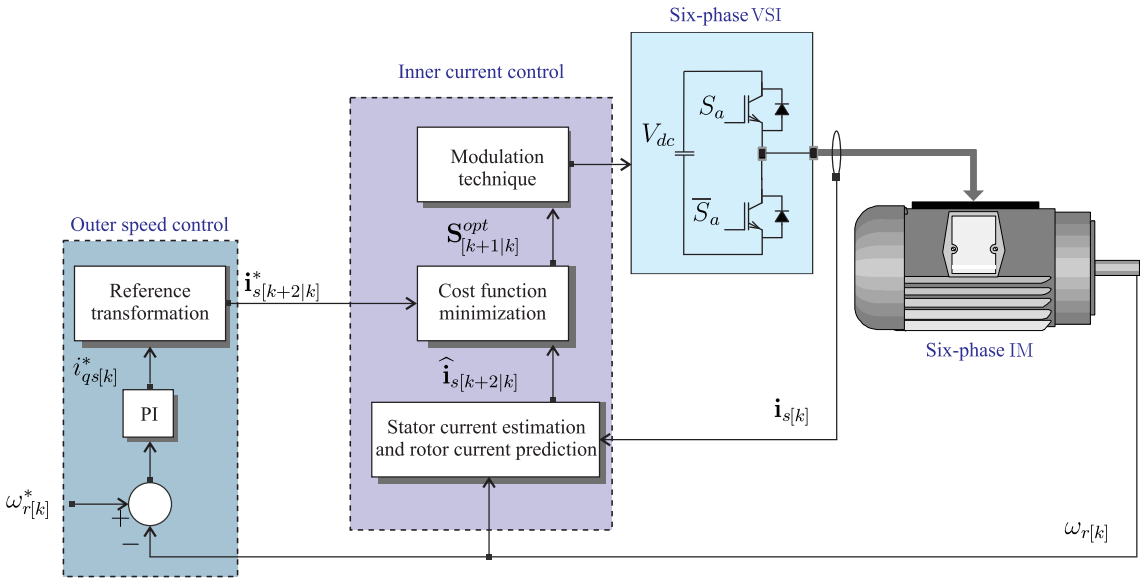

Fig. 3. Speed control with an inner current control based on predictive-fixed control and using KF for rotor current estimation.

Considering these expressions, the new cost function, which is evaluated at every T_s, is defined as:

$$G_{[k+2|k]} = d_1 J_1 + d_2 J_2 \tag{19}$$

The two vectors which minimize $G_{[k+2|k]}$ are selected and applied to the VSI at the next sampling time. After obtaining the duty cycles and selecting the optimal two vectors to be applied, a switching pattern procedure, shown in [15], is adopted with the goal of applying the two active vectors $(v_1 - v_2)$ and two zero vectors (v_0), considering the calculated duty cycles obtaining a fixed-switching frequency.

IV. Experimental Results

A detailed block diagram of the MPC technique for the six-phase IM is provided in Fig. 3. The six-phase IM is powered by two typical three-phase VSI, using a constant DC voltage of 400 V from a DC power supply. The VSI are controlled by a dSPACE MABXII DS1401 real-time prototyping platform. The experimental results are captured and processed using MATLAB R2013b. The motor position is measured with a 1024-pulses-per-revolution incremental encoder, and then, the speed is estimated from it. A 5 HP eddy current brake is used to connect a variable mechanical load. Table I shows the electrical and mechanical parameters for the six-phase IM.

TABLE I
Electrical and Mechanical Parameters of the six-phase IM

R_r	6.9 Ω	L_s	654.4 mH
R_s	6.7 Ω	P	1
L_{ls}	5.3 mH	P_w	2 kW
L_{lr}	12.8 mH	J_i	0.07 kg.m^2
L_m	614 mH	B_i	0.0004 kg.m^2/s
L_r	626.8 mH	ω_{r-nom}	3000 rpm

In Table II and Table III, a steady state analysis for stator currents under different rotor speed references (ω^*_r), are shown with M2PC and classic MPC, respectively. A total of 7 samples are obtained to measure the MSE for (α-β), (x-y) stator currents and the mechanical rotor speed (ω_r) as well as the THD for (α-β) stator currents.

TABLE II
Analysis of N Samples of Stator Currents (α-β), (x-y), MSE [A], THD [%] for M2PC at Different Rotor Speeds [rpm].

		Speed	ω^*_r =	500	[rpm]		
N	MSE$_\alpha$	MSE$_\beta$	MSE$_x$	MSE$_y$	THD$_\alpha$	THD$_\beta$	MSE$_{\omega_r}$
1	0.1140	0.1226	0.1662	0.2060	10.7	9.6	1.9233
2	0.1210	0.1199	0.1508	0.2037	10.5	9.5	1.6378
3	0.1151	0.1207	0.1653	0.2084	10.7	9.4	1.8141
4	0.1233	0.1183	0.1458	0.1981	11.0	9.7	1.8051
5	0.1171	0.1141	0.1529	0.1969	10.1	8.8	1.6634
6	0.1196	0.1158	0.1590	0.1958	10.3	9.0	1.8145
7	0.1111	0.1184	0.1691	0.2027	10.6	9.5	1.5835
		Speed	ω^*_r =	1000	[rpm]		
N	MSE$_\alpha$	MSE$_\beta$	MSE$_x$	MSE$_y$	THD$_\alpha$	THD$_\beta$	MSE$_{\omega_r}$
1	0.1546	0.1470	0.1644	0.2615	12.4	9.9	2.3932
2	0.1491	0.1432	0.1761	0.2599	12.3	9.7	2.6218
3	0.1583	0.1465	0.1677	0.2648	12.3	9.7	2.3217
4	0.1596	0.1480	0.1666	0.2630	12.5	9.9	2.3814
5	0.1594	0.1487	0.1797	0.2650	12.0	9.7	2.6432
6	0.1508	0.1487	0.1807	0.2685	12.0	10.0	2.7061
7	0.1487	0.1485	0.1771	0.2656	12.6	9.9	2.3885
		Speed	ω^*_r =	1500	[rpm]		
N	MSE$_\alpha$	MSE$_\beta$	MSE$_x$	MSE$_y$	THD$_\alpha$	THD$_\beta$	MSE$_{\omega_r}$
1	0.2044	0.1895	0.1875	0.3331	17.5	11.7	3.5112
2	0.2182	0.1908	0.1864	0.3199	18.0	12.1	2.9387
3	0.2193	0.1938	0.1820	0.3220	18.6	12.6	3.2329
4	0.2068	0.1921	0.1863	0.3204	17.8	12.0	2.9350
5	0.2197	0.1909	0.1920	0.3131	17.5	12.0	3.0535
6	0.2106	0.1926	0.1953	0.3277	17.1	12.0	3.2980
7	0.2094	0.1924	0.1907	0.3350	18.3	12.2	2.9544

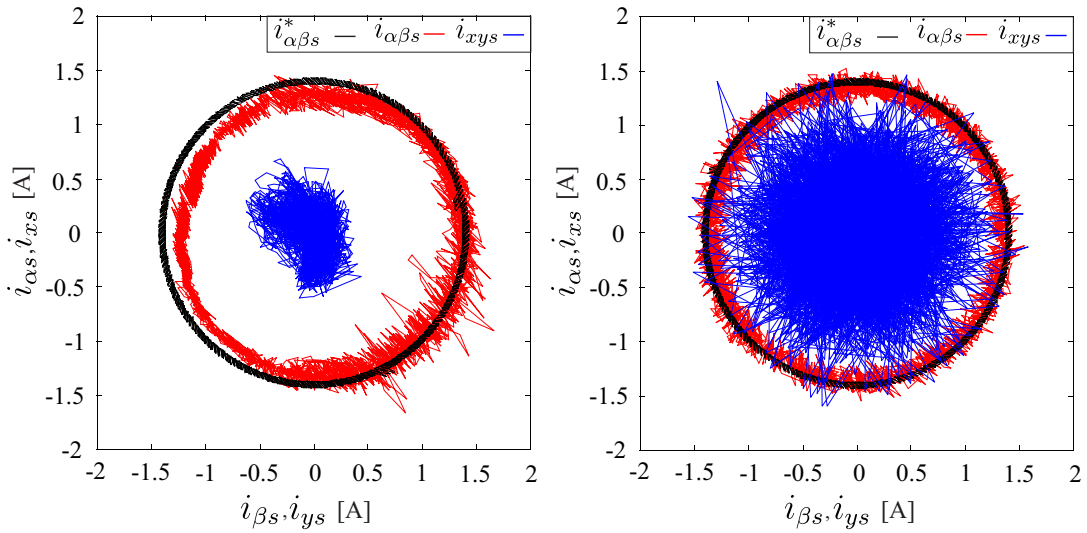

Fig. 4. Stator currents in (α-β) and (x-y) sub-spaces for rotor speed of 500 [rpm] and a sampling frequency of 16 [kHz]: (a) Amplitude of 1.5 [A] for M2PC; (b) Amplitude of 1.5 [A] for classic MPC.

TABLE III
ANALYSIS OF N SAMPLES OF STATOR CURRENTS (α-β), (x-y), MSE [A], THD [%] FOR CLASSIC MPC AT DIFFERENT ROTOR SPEEDS [RPM].

		Speed	ω_r^* =	500	[rpm]		
N	MSE_α	MSE_β	MSE_x	MSE_y	THD_α	THD_β	MSE_{ω_r}
1	0.0730	0.0719	0.4849	0.4929	8.3	8.3	1.7649
2	0.0713	0.0718	0.4825	0.4729	8.3	8.3	1.7851
3	0.0717	0.0713	0.4766	0.4771	8.5	8.2	1.9413
4	0.0726	0.0710	0.4868	0.4791	8.4	8.3	1.6323
5	0.0728	0.0713	0.4839	0.4800	8.5	8.3	1.9156
6	0.0731	0.0722	0.4835	0.4868	8.1	8.3	1.6481
7	0.0731	0.0726	0.4911	0.4839	8.2	8.0	1.6629
		Speed	ω_r^* =	1000	[rpm]		
N	MSE_α	MSE_β	MSE_x	MSE_y	THD_α	THD_β	MSE_{ω_r}
1	0.0847	0.0837	0.5332	0.5322	7.4	7.3	2.1235
2	0.0851	0.0827	0.5298	0.5407	7.5	7.1	2.2418
3	0.0841	0.0808	0.5386	0.5408	7.4	7.1	2.2721
4	0.0848	0.0813	0.5405	0.5327	7.4	7.2	2.1209
5	0.0845	0.0833	0.5356	0.5326	7.4	7.4	1.9444
6	0.0830	0.0822	0.5434	0.5340	7.3	7.3	2.1001
7	0.0844	0.0827	0.5385	0.5347	7.5	7.3	2.1238
		Speed	ω_r^* =	1500	[rpm]		
N	MSE_α	MSE_β	MSE_x	MSE_y	THD_α	THD_β	MSE_{ω_r}
1	0.0720	0.0706	0.5283	0.5144	7.0	6.9	3.0061
2	0.0726	0.0728	0.5190	0.5214	7.0	7.0	3.1270
3	0.0726	0.0703	0.5211	0.5101	7.6	6.9	2.9781
4	0.0706	0.0721	0.5238	0.5180	6.8	6.6	2.7550
5	0.0727	0.0727	0.5328	0.5241	7.0	6.8	3.1873
6	0.0720	0.0703	0.5239	0.5221	6.9	6.7	2.9386
7	0.0682	0.0698	0.5180	0.5134	6.8	6.7	2.5484

TABLE IV
EFFICIENCY ANALYSIS OF BOTH CONTROLLERS BASED ON STATISTICAL TEST.

AH1:	M2PC/Speed	AH2:	Classic MPC/Speed
Variables	p-value	Variables	p-value
MSE_α	0.001	MSE_α	0.001
MSE_β	0.001	MSE_β	0.001
MSE_x	0.001	MSE_x	0.001
MSE_y	0.001	MSE_y	0.001
THD_α	0.001	THD_α	0.001
THD_β	0.001	THD_β	0.001
MSE_{ω_r}	0.001	MSE_{ω_r}	0.001
AH3:	M2PC/Classic MPC 500 [rpm]	AH4:	M2PC/Classic MPC 1500 [rpm]
Variables	p-value	Variables	p-value
MSE_α	0.002	MSE_α	0.001
MSE_β	0.002	MSE_β	0.001
MSE_x	0.002	MSE_x	0.001
MSE_y	0.002	MSE_y	0.001
THD_α	0.002	THD_α	0.001
THD_β	0.001	THD_β	0.001
MSE_{ω_r}	0.949	MSE_{ω_r}	0.259

Fig. 4 exposes the (α-β) and (x-y) stator currents tracking, for M2PC and classic MPC, in steady state for the rotor speed. Fig. 5 shows the transient response for q stator current in a reversal test (speed reference changes from 500 [rpm] to -500 [rpm]) where the M2PC and classic MPC show similar response speed. The presented results in Table IV were obtained by the Mann-Whitney non-parametric statistical test using the software SPSS version 20.0. AH1 is a alternative hypothesis where the variables (MSE and THD) equality is verified for M2PC at different rotor speeds (500 [rpm] and 1000 [rpm]). By considering the obtained probability value (p-value) it can be deducted that the M2PC efficiency is better for a rotor speed of 500 [rpm] in comparison to 1000 [rpm]. After processing other data revolving different rotor speeds, it is obtained a similar result where M2PC has better performance with lower rotor speeds. AH2 is defined as the same analysis than AH1 for classic MPC, where the results are the same, a better performance at lower speed. AH3 and AH4

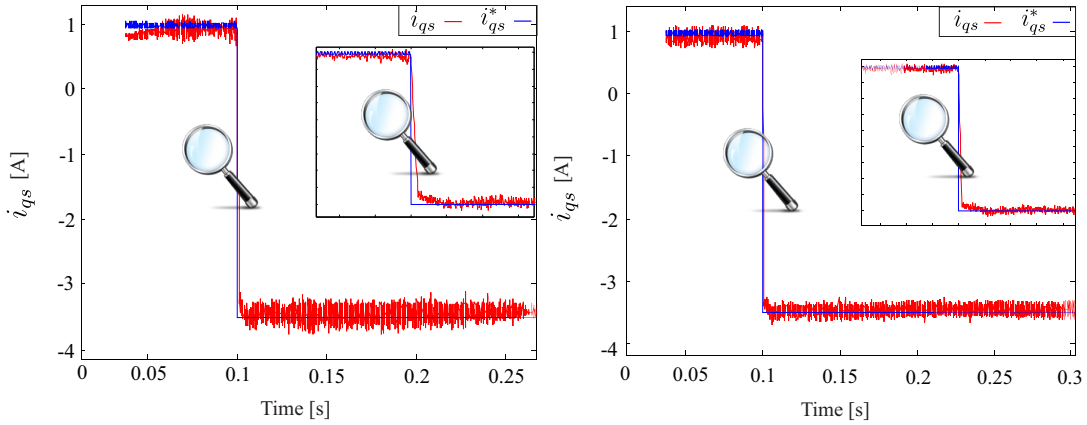

Fig. 5. Transient response in q-axis stator current for rotor speed of 500 [rpm] to -500 [rpm] and a sampling frequency of 16 [kHz]: (a) For M2PC; (b) For classic MPC.

are alternative hypothesis that compare the efficiency of both techniques (M2PC and classic MPC) at rotor speeds of 500 and 1500 [rpm], respectively. The registered p-values demonstrate a different efficiency, particularly better for classic MPC over M2PC in terms of MSE_α, MSE_β, THD_α and THD_β. While M2PC efficiency is far superior for MSE_x and MSE_y. On the other hand, for MSE_{ω_r} the p-value shows that there is not sufficient statistical evidence to reject the same efficiency for both techniques.

V. Conclusion

In this paper a variable-speed control with a modified predictive current control technique with fixed switching frequency (M2PC) applied to the six-phase IM is presented. The experimental and statistical results were compared between M2PC and the classic MPC and showed a better performance in the (x-y) currents reduction for M2PC. However, in the (α-β) currents tracking, M2PC had a worse performance compared to classic MPC due to a saturation effect in the measured currents. In terms of speed tracking both techniques had similar results and in the transient analysis, the response was almost the same for both techniques. It can be concluded that M2PC is a good alternative to classic MPC to improve the (x-y) currents reduction.

Acknowledgment

The authors wish to thank the financial support from the Paraguayan Science and Technology National Council (CONACYT) through project 14-INV-101.

References

[1] E. Levi, "Advances in converter control and innovative exploitation of additional degrees of freedom for multiphase machines," *IEEE Trans. Ind. Electron.*, vol. 63, no. 1, pp. 433–448, 2016.

[2] I. Subotic, N. Bodo, and E. Levi, "Integration of six-phase EV drivetrains into battery charging process with direct grid connection," *IEEE Trans. Energy Convers.*, vol. 32, no. 3, pp. 1012–1022, 2017.

[3] M. Ayala, O. Gonzalez, J. Rodas, R. Gregor, and J. Doval-Gandoy, "A speed-sensorless predictive current control of multiphase induction machines using a Kalman filter for rotor current estimator," in *Proc. ESARS-ITEC*, pp. 1–6, 2016.

[4] M. Jones, S. N. Vukosavic, D. Dujic, and E. Levi, "A synchronous current control scheme for multiphase induction motor drives," *IEEE Trans. Energy Convers.*, vol. 24, no. 4, pp. 860–868, 2009.

[5] H. S. Che, M. J. Duran, E. Levi, M. Jones, W.-P. Hew, and N. A. Rahim, "Postfault operation of an asymmetrical six-phase induction machine with single and two isolated neutral points," *IEEE Trans. Power Electron.*, vol. 29, no. 10, pp. 5406–5416, 2014.

[6] S. Vazquez, J. Rodriguez, M. Rivera, L. G. Franquelo, and M. Norambuena, "Model predictive control for power converters and drives: Advances and trends," *IEEE Trans. on Ind. Electron.*, vol. 64, no. 2, pp. 935–947, 2016.

[7] M. Vijayagopal, P. Zanchetta, L. Empringham, L. De Lillo, L. Tarisciotti, and P. Wheeler, "Modulated model predictive current control for direct matrix converter with fixed switching frequency," in *Proc. EPE*, 2015, pp. 1–10, 2015.

[8] F. Gavilan, D. Caballero, S. Toledo, E. Maqueda, R. Gregor, J. Rodas, M. Rivera, and I. Araujo-Vargas, "Predictive power control strategy for a grid-connected 2L-VSI with fixed switching frequency," in *Proc. ROPEC*, pp. 1–6, 2016.

[9] S. Toledo, M. Rivera, J. Muñoz, R. Peña, J. Riveros, and R. Gregor, "Fixed switching frequency predictive control for a multi-drive indirect matrix converter system," in *Proc. SPEC*, pp. 1–6, 2017.

[10] M. Rivera, S. Toledo, C. Baier, L. Tarisciotti, P. Wheeler, and S. Verne, "Indirect predictive control techniques for a matrix converter operating at fixed switching frequency," in *Proc. PRECEDE*, pp. 13–18, 2017.

[11] L. Comparatore, R. Gregor, J. Rodas, J. Pacher, A. Renault, and M. Rivera, "Model based predictive current control for a three-phase cascade H-bridge multilevel STATCOM operating at fixed switching frequency," in *Proc. PEDG*, pp. 1–6, 2017.

[12] L. Harnefors, S. Saarakkala, and M. Hinkkanen, "Speed control of electrical drives using classical control methods," *IEEE Trans. Ind. Appl.*, vol. 49, no. 2, pp. 889–898, 2013.

[13] H. B. Mann and D. R. Whitney, "On a test of whether one of two random variables is stochastically larger than the other," *The annals of mathematical statistics*, pp. 50–60, 1947.

[14] Y. Zhao and T. Lipo, "Space vector PWM control of dual three-phase induction machine using vector space decomposition," *IEEE Trans. Ind. Electron.*, vol. 31, no. 5, pp. 1100–1109, 1995.

[15] M. Ayala, J. Rodas, R. Gregor, J. Doval-Gandoy, O. Gonzalez, M. Saad, and M. Rivera, "Comparative study of predictive control strategies at fixed switching frequency for an asymmetrical six-phase induction motor drive," in *Proc. IEMDC*, pp. 1–8, 2017.

[16] J. Rodas, F. Barrero, M. R. Arahal, C. Martin, and R. Gregor, "On-line estimation of rotor variables in predictive current controllers: A case study using five-phase induction machines," *IEEE Trans. Ind. Electron.*, vol. 63, no. 9, pp. 5348–5356, 2016.

[17] J. Rodas, C. Martin, M. R. Arahal, F. Barrero, and R. Gregor, "Influence of covariance-based ALS methods in the performance of predictive controllers with rotor current estimation," *IEEE Trans. Ind. Electron.*, vol. 64, no. 4, pp. 2602–2607, 2017.